Japanese Journal of Applied Physics

REGULAR PAPER

A new evaluation method for dependence of width of transmitted waves on accuracy in multipoint simultaneous ultrasonic measurements of cardiac wall vibration waveform

Japanese Journal of Applied Physics **58**, SGGA08 (2019) **REGULAR PAPER**
https://doi.org/**10.7567/1347-4065/ab1a30**

A new evaluation method for dependence of width of transmitted waves on accuracy in multipoint simultaneous ultrasonic measurements of cardiac wall vibration waveform

Naoya Furusawa[1], Shohei Mori[2*], Mototaka Arakawa[1,2], and Hiroshi Kanai[2,1]

[1]*Graduate School of Biomedical Engineering, Tohoku University, Sendai, Miyagi 980-8579, Japan*
[2]*Graduate School of Engineering, Tohoku University, Sendai, Miyagi 980-8579, Japan*

[*]E-mail: mori@ecei.tohoku.ac.jp

Received November 9, 2018; accepted March 30, 2019; published online June 28, 2019

It has been revealed that the ultrasound measurement with high temporal resolution is useful for diagnosis of myocardial tissue properties. However, it is considered that the dynamic measurement of the target tissue is affected by the motion of neighbor tissues because of the wide width of the transmitted wave. For this reason, the measurement error is affected by spatial and temporal factors. In the present study, we constructed an experimental system for measuring these effects quantitatively and investigated the accuracy of the velocity measurement using some transmitted waves such as focused, plane, and diverging waves. In the conditions of the present study, the measurement error is minimized at 9° of the angular width of the transmitted wave. This method is useful for evaluating the conditions of transmitted waves for measurements of other targets which need a high temporal resolution such as shear wave, cardiac blood flow, and so on.

1. Introduction

As ultrasound diagnosis is superior in a temporal resolution and suitable for repetitive application, it has been widely applied to measurements in the living body such as elastography on the heart or artery wall,[1–3] blood flow in the heart,[4–7] visualization of the shear wave,[8,9] measurement of propagation of contraction or electrical signal on myocardium,[10–14] and so on. The experimental environment to be simulated is decided by the specific measurement target from the above measurements. If it is possible to determine the transmission condition that minimizes the measurement error for the measurement object whose true value is known, it is expected that the optimum measurement condition can also be shown even in the in vivo experiment where the true value is unknown.

Myocardial tissue functions can be evaluated by the propagation speed of minute vibration velocity waveforms within the maximum velocity of 60 mm s^{-1} on the heart wall acquired with high-frame-rate imaging using sparsely transmitted focused waves.[15–17] As the other technique to improve the temporal resolution, it had been proposed that an unfocused wave is transmitted and multiple focused receiving beams are created from received signals by plural elements of the ultrasonic probe.[18–23] As this method increases the spatial resolution by forming the received beams with high density, it was applied to strain measurements at multiple points in the heart wall.[24]

As mentioned above, a high temporal resolution is required for dynamic measurements of the heart, so many researches in cardiac ultrasound are focused on improving the temporal resolution. However, by broadening the width of the transmitted wave spatially, the spatial resolution and signal-to-noise ratio (SNR) are, in general, degraded. Moreover, it is considered that the dynamic measurement of the target tissue is affected by the motion of the neighbor tissues. Therefore, high spatial and temporal resolutions with high SNR are needed for the dynamic measurement of the heart, while there is a trade-off relationship among the temporal resolution, the spatial resolution in the minute vibration velocity measurement, and the SNR. The trade-off relationship between the image quality and the frame rate has been investigated using a static target.[25] However, the measurement accuracy of the minute vibration velocity in a moving target has not been investigated considering the trade-off relationship among the temporal resolution, the spatial resolution in the minute vibration velocity measurement, and the SNR.

In a previous study, we constructed a basic experiment system to evaluate the relationship between the condition of transmitted waves and the accuracy of the minute vibration velocity measurements.[26] However, the evaluation method for optimum condition of transmitted waves considering the above trade-off relationship was not established. In addition, the examined experimental conditions were insufficient to determine the optimum condition of transmitted waves for minute vibration velocity measurements.

In the present study, all transmitted wave conditions of focused, plane, and diverging waves were expressed uniformly by a single parameter, then we proposed an evaluation method of the accuracy of the minute vibration velocity measurement in each transmitted wave condition depending on the above trade-off relationship. We constructed the basic experimental system with setting several conditions to measure the minute vibration velocity waveform propagating on the interventricular septum[15] and demonstrated the quantitative evaluation of the accuracy of measuring the minute vibration velocity as a method for determining the optimum condition of transmitted waves.

2. Methods

2.1. Evaluation method for measurement accuracy considering trade-off relationship

In the present study, we consider the measurement of the vibration waveform. Therefore, it is necessary to consider not the mere spatial resolution but the spatial resolution of the minute vibration velocity measurement which means the distance not to be affected by neighbor vibrations whose velocity differs from the velocity of measurement target. Then, we constructed an experimental system to investigate

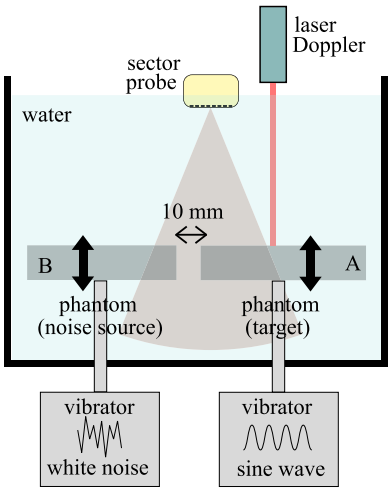

Fig. 1. (Color online) Configuration of the experimental system.

the influence on accuracy of the vibration velocity measurement as shown in Fig. 1.

To evaluate the spatial resolution in the velocity measurement, two phantoms A and B were used as shown in Fig. 1. The phantom B was set near the measurement target phantom A as a neighbor vibration object whose velocity differs from the velocity of the measurement target. It is expected that measurement error α increases by the influence of the reflected waves from phantom B when the diverging wave is transmitted for the velocity measurement. The main objective of this research is to evaluate the performance of the vibration measurement against the influence of the surrounding vibrations under some transmission conditions, so it is not desirable that the vibrations interfere with each other on the phantom. Therefore, in the present paper, the target of the velocity measurement (phantom A) and a neighbor vibration object (phantom B) were spaced and independently vibrated.

In this water tank experimental system, the vibration velocity waveform $\widehat{v_{\mathrm{U}}}(n)$ of phantom A was measured by ultrasound diagnosis equipment using a phased-tracking method,[27,28] and the vibration velocity waveform $v_{\mathrm{L}}(n)$ was also measured by laser Doppler velocimetry as a reference. To evaluate the accuracy of the vibration velocity, the measurement error of the vibration waveform, α, was defined as

$$\alpha = \frac{\sqrt{\sum_{n=0}^{N-1}\{\widehat{v_{\mathrm{U}}}(n) - v_{\mathrm{L}}(n)\}^2}}{\sqrt{\sum_{n=0}^{N-1}\{v_{\mathrm{L}}(n)\}^2}}, \tag{1}$$

where N is the number of frames, and n is frame number.

Thus, the measurement accuracy of the velocity waveform can be quantitatively evaluated with considering the trade-off relationship among the temporal resolution, the spatial resolution in the velocity measurement, and the SNR in the present experimental system.

2.2. Expression of transmitted wave conditions with a single parameter

To express the condition of transmitted waves such as focused, plane, and diverging waves, we defined the angular width θ_{w}. The angular width θ_{w} was introduced in the previous study to express the unfocused wave condition.[2]

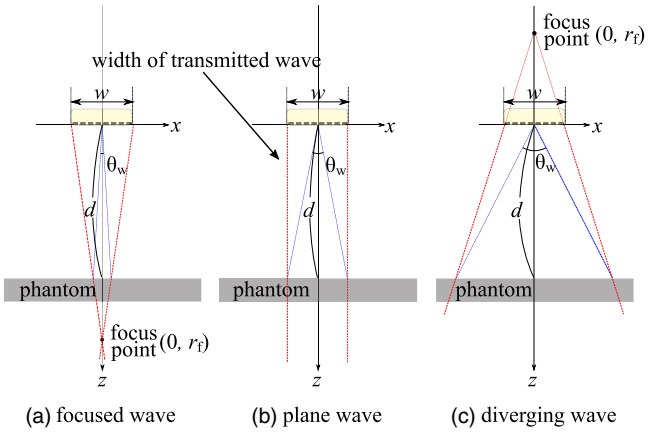

Fig. 2. (Color online) Definition of angular width θ_{w} of (a) focused wave, (b) plane wave, and (c) diverging wave.

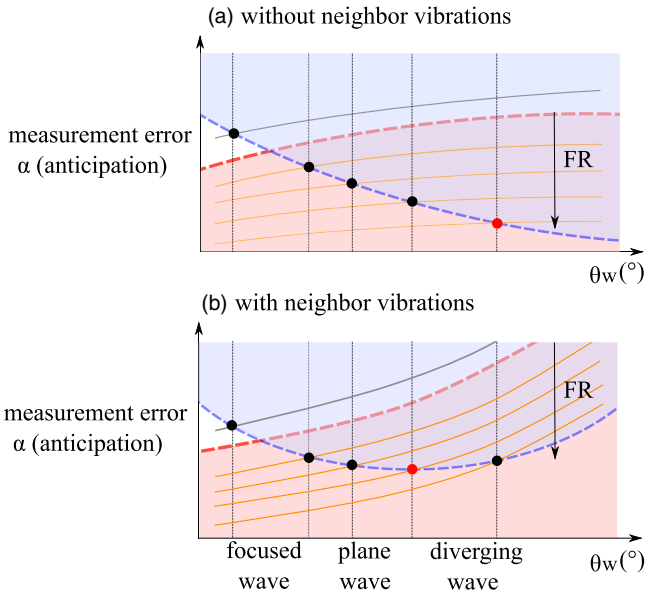

Fig. 3. (Color online) The anticipation of measurement error of minute vibration velocity (a) without neighbor vibrations, (b) with neighbor vibrations.

In the present study, we expanded the definition of the angular width θ_{w} to the focused wave to express all transmitted wave conditions only by a single parameter θ_{w}. The angular width θ_{w} was defined as

$$\theta_{\mathrm{w}} = 2\tan^{-1}\left(w\frac{r_{\mathrm{f}} - d}{2r_{\mathrm{f}}d}\right), \tag{2}$$

where r_{f} is depth of focal point, w is aperture width, and d is target depth.

As shown in Fig. 2, r_{f} of the focused wave is a positive number (front side of the probe surface), and r_{f} of the diverging wave is a negative number (virtual point source). In the case of the plane wave, the focal point is at infinity and θ_{w} is 22° under the experimental condition. In the present study, the focal depth of the transmitted wave with $\theta_{\mathrm{w}} = 20°$ was 458 mm, which was thought to be far enough, it was dealt with as a plane wave.

2.3. Anticipation of measurement error

We predict the measurement error α for measurements of the minute vibration velocity waveform propagating on the ventricular septal wall as the schematic view shown in Fig. 3.

Figure 3(a) shows the case where there is no neighbor object. On the other hand, Fig. 3(b) shows the case where there is a neighbor object whose velocity differs from that of the measurement target.

Each orange and gray line in Fig. 3 shows the measurement error α for the change of the angular width θ_w under the same frame rate. In this case, it is expected that the measurement error of the vibration velocity will decrease, since the SNR increases as the width of the transmitted wave is narrower. The larger the θ_w is, the more gradual the change in SNR. Thus, the measurement error prediction curve in Fig. 3(a) is considered to be convex upward for the change in angular width. On the other hand, in the case of Fig. 3(b), it is considered that the larger θ_w is affected by the surrounding vibrations. Therefore, the measurement error prediction curve is considered to be downward convex.

In the phased-tracking method, the maximum velocity measured without aliasing is determined by the frame rate in the measurement. Therefore, when the velocity of an object vibrating with various velocity components is measured by the phased-tracking method, velocities higher than the upper limit of the velocity cannot be accurately measured. As a result, as the frame rate decreases, the measurement error increases.

The minimum frame rate FR_{MIN} required to avoid aliasing is expressed as

$$FR_{MIN} = |v_{MAX}| \frac{4f_0}{c_0}, \tag{3}$$

where $|v_{MAX}|$ is the absolute value of maximum velocity, f_0 is the transmission frequency, and c_0 is the sound velocity. The anticipated errors of the vibration velocity measurement at the lower limit frame rate FR_{MIN} are shown by the red dotted lines in Fig. 3. Measurement errors at a frame rate larger than the lower limit of the frame rate are indicated by the red region. The orange solid lines are located lower than the red dotted line and have a sufficient frame rate for the measurement of the vibration velocity. The gray solid line is located higher than the dotted red line, so it has an insufficient frame rate for the measurement of the vibration velocity.

On the other hand, as the transmission beam width is narrower, the range of the vibration measurement per one transmission becomes narrower, so that the number of transmissions required for one frame increases. As a result, assuming a certain range of sector scanning, the maximum frame rate for the minute vibration velocity measurement decreases. Figure 4 shows a sector scan with the scanning angle of the transmitted beam $\Delta\theta$ and the measurement range θ_0. In this condition, if the transmission direction is tilted beyond the transmission beam width, a region where a high-intensity transmission wave does not reach is generated. In order to avoid the generation of this area, we set the range of $\Delta\theta$ as $\Delta\theta \leq \theta_w$. Then, the reachable frame rate FR_{MAX} is maximum when $\Delta\theta = \theta_w$, and it is determined by the beam width. The relationship between FR_{MAX} and θ_w is expressed as

$$FR_{MAX} = f_{PRF} \cdot \frac{\theta_w}{\theta_0}. \tag{4}$$

The maximum frame rate is indicated by a blue dotted line, and the measurable region is highlighted in blue in Fig. 3.

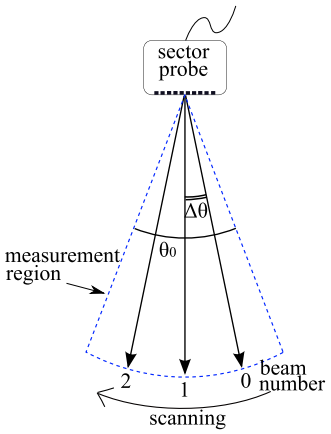

Fig. 4. (Color online) The scan by tilt angle $\Delta\theta$ and the angular range θ_0 of the field of view.

Therefore, the region satisfying Eqs. (3) and (4) is effective for the vibration velocity measurement.

Because θ_w is the angular width of the transmitted beam, the reachable upper frame rate can be determined assuming the sector scanning for cardiac measurement. However, in the case where the object to be measured is a shear wave for elastography in such as the liver, muscle, breast, and so on, the linear scan is used rather than the sector scan. Therefore, in order to specify the reachable upper frame rate for the linear scan, it is necessary to prepare another reasonable expression to associate the frame rate and the beam width.

It is considered that θ_w [red point in Fig. 3(a)] at which the error is the smallest in the case that there is neighbor vibration is smaller than that in the case there is no neighbor vibration [red point in Fig. 3(b)]. Therefore, θ_w at the minimum measurement error changes due to the influence of the neighbor vibration.

2.4. Water tank experiments

The experimental system was introduced to observe the minute vibration velocity waveform caused by changes of θ_w described in the previous section. The experimental configuration is shown in Fig. 1. RF data were acquired by the ProSound-SSD α10 (Aloka) with a sector probe (UST-52101N, Aloka) of 3.75 MHz of the transmission frequency. The laser Doppler velocimetry (LV-1300, Ono Sokki) was used as the reference. In the case of ultrasound measurement, received beams were formed in the range of ±21° using RF data acquired by one transmitted wave perpendicular to the probe surface. Minute vibration velocity waveforms were obtained from a center received beam (0°) using the phased-tracking method. Measurement errors α in Eq. (1) were calculated from the velocity waveform for 167 ms (5 wavelengths of 30 Hz).

The measurement of the propagation speed of the minute vibration velocity waveform on the heart wall caused by the myocardial contraction enables evaluation of myocardium function.[15] For measuring the propagation speed of myocardial contraction on the intervascular septum avoiding the influence of aliasing, we decided a spatial measurement interval without causing aliasing even at the shortest wavelength of propagation speed. In the previous study, the propagation speeds of contraction during avascularization condition and normal condition were approximately 1.6–3.6 m s^{-1}. Propagations of contraction responses on the

intervascular septum were analyzed at 10–90 Hz where they can be observed with high SNR.[19,29] Here, the wavelength of the propagation wave was calculated as approximately 20 mm from the minimum velocity of 1.6 m s^{-1} and with a frequency of 80 Hz. Therefore, in the present study, two phantoms were spaced 10 mm corresponding to the half of the wavelength to simulate the same movement on the phantom.

Phantom A, which is the measurement target, was vibrated up and down with the sine wave at 30 Hz and the maximum velocity of approximately 40 mm s^{-1} by a shaker A considering the minute vibration velocity waveform on the interventricular septum.[1] In the phased-tracking method, in order to accurately measure the vibration at the maximum velocity of 40 mm s^{-1}, a frame rate of about 400 Hz is necessary when the transmission frequency is 3.75 MHz. In the present study, the velocity waveform was measured with frame rates of 1,683 Hz and 561 Hz to satisfy this condition.

A white noise was input to the shaker connected to phantom B to quantitatively evaluate the influence of neighbor vibrations whose velocity differs from the measurement target. Although the frequency band of the input noise can be changed freely, we chose the white noise as the input noise for the demonstration experiment simulating the velocity measurement with neighbor vibrations because it is widely used as a background noise. The rms amplitude of the velocity input to shaker B was set to be a half value compared with that of shaker A. Considering the depth of the interventricular septum, two phantoms were set approximately 50 mm from the surface of the probe.

3. Results and discussion

Figure 5 shows B-mode images acquired by the transmitted wave with an angular width of (a) $\theta_w = 9°$ (focused wave), (b) $\theta_w = 20°$ (plane wave) and (c) $\theta_w = 61°$ (diverging wave), respectively. As shown in Fig. 5(c), in the case of a diverging wave, phantom A looked blurry which was caused by the effect of a reflected wave from phantom B because of its wide width of a transmitted wave.

Figure 6 shows an example of a waveform of the center received beam in the depth direction used for the velocity measurement. Large amplitudes were observed on the anterior and posterior surface of phantom A. The vibration velocity at the anterior surface was analyzed.

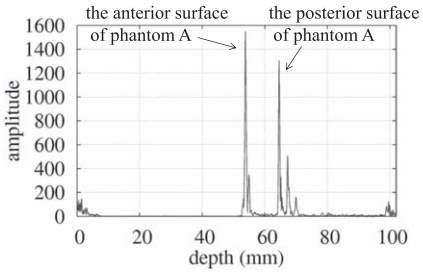

Fig. 6. An example of the waveform of the central receive beam.

Figure 7 shows the minute vibrated velocity waveforms acquired by the transmitted wave with angular width of (a) $\theta_w = 9°$ (focused wave), (b) $\theta_w = 20°$ (plane wave) and (c) $\theta_w = 61°$ (diverging wave), respectively. Except for focused waves of $\theta_w = 9°$, the amplitude of the velocity waveform measured by the ultrasound tended to be larger than that of the velocity waveform measured by the laser Doppler velocimetry. As the frame rate increased, the amplitude of the velocity waveform measured by the ultrasound increased. That also increased as θ_w increased.

Figure 8 shows measurement errors calculated by Eq. (1) on each transmitted wave condition. The blue dotted line expresses the angular width of the ideal plane wave. In these experimental conditions, as the measurement error was lowest at $\theta_w = 9°$, this transmitted wave condition was evaluated as the best transmission condition among the parameters shown in Table I. In terms of the diverging wave, the measurement errors in the case with phantom B was larger than those in the case without phantom B. Therefore, it was confirmed that the influence of neighbor vibrations increased as the beam width became wider. Furthermore, in all graphs, the measurement error at $\theta_w = 61°$ became larger than the measurement error at $\theta_w = 30°$. It is considered that the increase of measurement error was caused by the decrease of SNR with an increase of the angular width of the transmitted wave.

By contrast, the measurement error tended to decrease as the frame rate was lower, contrary to the anticipation. This is because the effect of reverberation in the water tank might increase as the frame rate became larger. This effect would be reduced by attaching an ultrasonic absorption material to the inner wall of the water tank. If we can confirm that the

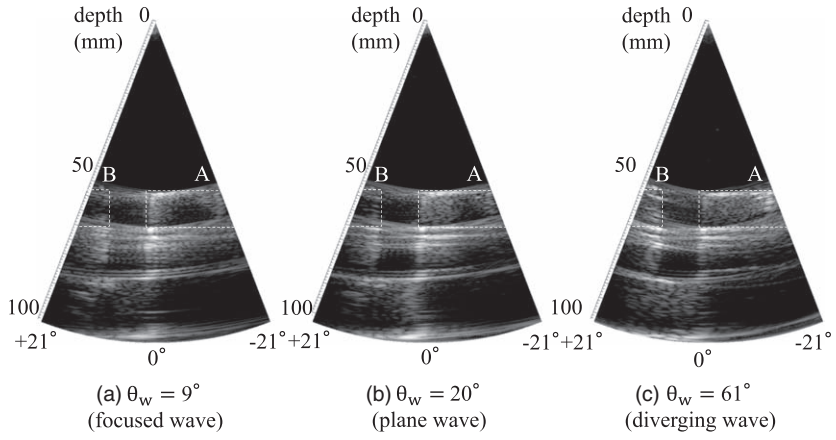

Fig. 5. B-mode images acquired by (a) focused wave, (b) plane wave, and (c) diverging wave.

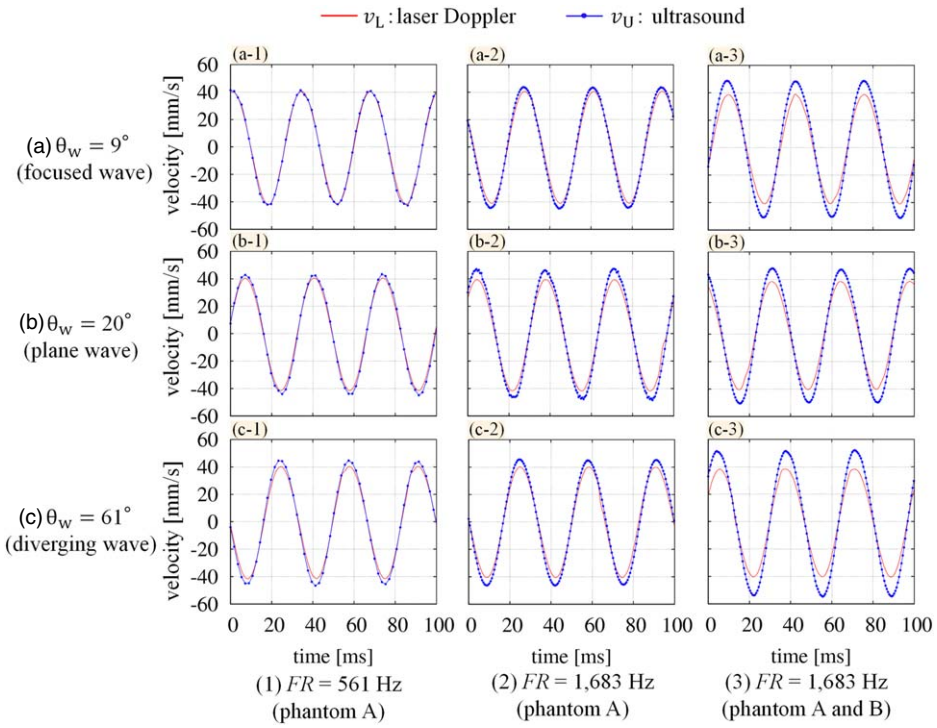

Fig. 7. (Color online) The velocity waveform measured by (a) focused wave, (b) plane wave, and (c) diverging wave.

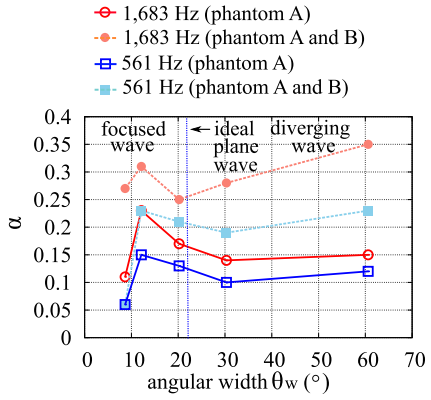

Fig. 8. (Color online) Angular width θ_W and the measurement error α of vibration velocity.

Table I. Transmission conditions.

r_f(mm)	80	107	458	−141	−26
θ_w(°)	9	12	20	30	61

measurement error increases as the frame rate decreases, the predicted measurement error curve (blue dotted line shown in Fig. 3) can be plotted from the measured values. Thus, it is considered that measurement conditions that minimize the measurement error can be specified.

At $\theta_w = 12°$ and 20° in Fig. 8, the measurement errors became larger than those with other angular widths, unlike the anticipation in Fig. 3. We will investigate the cause because the cause is unknown at the moment.

A deviation in the transmission frequency might be considered as a cause of the amplitude of the velocity waveform not matching between the laser measurement and the ultrasonic measurement even in the absence of phantom B. When the transmission frequency adopted for the velocity measurement in the phased-tracking method is deviated from the center frequency of the received waveform, the amplitude of the estimated velocity waveform is affected. In order to eliminate this effect, a proper transmission frequency must be determined to calculate the velocity waveform. This specification method needs to be examined in the future.

The object of measurement in the present study is a minute vibration velocity waveform propagating on myocardium. In the previous study,[15–17] the minute vibration velocity waveform was calculated at plural points on the cardiac muscle, and the propagation speed of these velocity waveforms was calculated by the cross correlation between them. As a result, it was confirmed that the propagation speed decreased in the ischemic conditions. However, there were measurement points where the correlation coefficients between the vibration velocity waveforms were low, and the dispersion of the estimated propagation speed was large. Higher correlation is desired in order to estimate the ischemic part more locally. By examining the relationship between the correlation of the minute velocity waveforms and the measurement accuracy, we believe that it is possible to specify the target value of the measurement error for the minute velocity waveform in the future.

If an acceptable measurement error can be specified concretely and the measurement error indicated by this method cannot achieve the target value, it is necessary to improve the beamforming method or the performance of signal processing after imaging.[30] Since the proposed method can evaluate quantitatively the measurement accuracy of the vibration velocity, this method is also effective for the evaluation of their performance.

In the case of a diverging wave, it was suggested that the artifact from phantom B interfered in the measurement of vibration velocity of phantom A and this interference caused an increase of measurement errors.

In this study, vibration frequency and maximum vibration velocity were selected as 30 Hz and 40 mm s^{-1}, respectively. On the other hand, in the case of a higher noise power emitted by phantom B and shorter interval between two phantoms, that of the wide transmitted wave would increase. In the present study, we investigated some particular cases. Therefore, there is a need for further investigation into various situations. However, the proposed method and the experimental system enables us to uniformly compare transmission conditions and quantitatively to evaluate errors of vibration velocity with variously changing measurement conditions such as vibration velocity, noise power, and distance between two phantoms. We have concluded that future works can seemingly reveal the condition of the minimum measurement error.

The present evaluation method can determine the suitable transmitted wave condition considering the trade-off relationship among the temporal resolution, the spatial resolution in the velocity measurement, and the SNR. Although the measurement target was set to the waveform of the minute vibration velocity on the heart wall in this paper, this method is useful to optimize the transmitted wave conditions for measurement of several targets which need a high temporal resolution such as elastography,[1–3] shear wave imaging,[8,9] and so on.

If the object to be measured is the blood flow in the heart, for example, by preparing a cardiac simulated phantom driven by an internal pressure change, in place of the object of the vibration measurement (phantom A) in this paper, it is considered that it is possible to decide a suitable transmission condition for the blood flow against the influence of neighbor vibrations. In addition, if the object to be measured is a shear wave, for example, by vibrating a part of the material close to the viscoelasticity of the living body using this experimental system, it is considered that it is possible to decide a suitable transmission condition for the measurement of a shear wave under the influence of neighbor vibrations.

4. Conclusions

For the determination of suitable transmitted wave conditions of ultrasound in the measurement of the minute vibration velocity waveform on the heart wall, we constructed an experimental system and proposed a method to evaluate the measurement accuracy considering the trade-off relationship among the temporal resolution, the spatial resolution in the velocity measurement, and the SNR, in several conditions of transmitted waves such as focused, plane, and diverging waves. From the water tank experiment, we demonstrated the determination of the suitable transmitted wave condition for measuring the minute vibration velocity waveform on the heart wall. The measurement errors of the vibration velocity would systematically change depending on the experimental conditions. Therefore, we will further investigate the errors in various cases. Moreover, we will reveal how noises from neighbor points affect the measurement accuracy. In the future, we plan to limit the excitation frequency of the phantom B to the reasonable frequency band in in vivo.

Acknowledgments

This work was partially supported by JSPS KAKENHI Grant No. 17H02105.

ORCID iDs

Shohei Mori https://orcid.org/0000-0002-5494-1055
Mototaka Arakawa https://orcid.org/0000-0001-9386-645X
Hiroshi Kanai https://orcid.org/0000-0002-6567-1687

1) T. Motonao, T. Sakamoto, S. Sugawara, Y. Katahira, K. Hasegawa, H. Nakajima, T. Kurokawa, H. Kanai, and H. Hasegawa, J. Cardiol. **69**, 462 (2017).
2) H. Hasegawa and H. Kanai, J. Med. Ultrason. **38**, 129 (2011).
3) D. P. Shattuck, M. D. Weinshenker, S. W. Smith, and O. T. von Ramm, J. Acoust. Soc. Am. **75**, 1279 (1986).
4) S. Ricci, L. Bassi, and P. Tortoli, IEEE Trans. Ultrason. Ferroelectr. Freq. Control **61**, 314 (2014).
5) M. Maeda, R. Nagaoka, H. Ikeda, S. Yaegashi, and Y. Saijo, Jpn. J. Appl. Phys. **57**, 07LF02 (2018).
6) S. Salles, A. J. Y. Chee, D. Garcia, A. C. H. Yu, D. Vray, and H. Liebgott, IEEE Trans. Ulrason. Ferroelectr. Freq. Control. **61**, 1047 (2015).
7) H. Takahashi, H. Hasegawa, and H. Kanai, Jpn. J. Appl. Phys. **53**, 07KF08 (2014).
8) L. Sandrin, S. Catheline, M. Tanter, X. Hennequin, and M. Fink, Ultrason. Imaging **21**, 259 (1999).
9) M. Tanter, J. Bercoff, L. Sandrin, and M. Fink, IEEE Trans. Ultrason. Ferroelectr. Freq. Control **49**, 1363 (2002).
10) G. R. Sutherland, G. D. Salvo, P. Claus, J. D'hooge, and B. Bijnens, J. Am. Soc. Echocardiogr. **17**, 788 (2004).
11) M. Dandel, H. Lehmkuhl, C. Knosalla, N. Suramelashvili, and R. Hetzer, Current Cardiol. Rev. **5**, 133 (2009).
12) M. Dandel and R. Hetzer, Int. J. Cardiol. **132**, 11 (2009).
13) R. Jasaityte and J. D'hooge, Imaging Med. **2**, 547 (2010).
14) Y.-F. Cheung, Nat. Rev. Cardiol. **9**, 644 (2012).
15) Y. Matsuno, H. Taki, H. Yamamoto, M. Hirano, S. Morosawa, H. Shimokawa, and H. Kanai, Jpn. J. Appl. Phys. **56**, 07JF05 (2017).
16) A. Hayashi, S. Mori, M. Arakawa, H. Yamamoto, S. Morosawa, H. Shimokawa, and H. Kanai, Proc. IEEE Int. Ultrasonics Symp., 2018 (http://doi.org/10.1109/ULTSYM.2018.8579780).
17) A. Hayashi, S. Mori, M. Arakawa, and H. Kanai, Jpn. J. Appl. Phys. **58**, SGGE05 (2019).
18) J. Provost, V. T.-H. Nguyen, D. Legrand, S. Okrasinski, A. Costet, A. Gambhir, H. Garan, and E. E. Konofagou, Phys. Med. Biol. **56**, L1 (2011).
19) H. Kanai, IEEE Trans. Ultrason. Ferroelectr. Freq. Control **52**, 1931 (2005).
20) H. Hasegawa and H. Kanai, IEEE Trans. Ultrason. Ferroelectr. Freq. Control **55**, 2626 (2008).
21) C. Papadacci, M. Pernot, M. Couade, M. Fink, and M. Tanter, IEEE Trans. Ultrason. Ferroelectr. Freq. Control **61**, 288 (2014).
22) M. Correia, J. Provost, S. Chatelin, O. Villemain, M. Tanter, and M. Pernot, IEEE Trans. Ultrason. Ferroelectr. Freq. Control **63**, 420 (2016).
23) J. Grondin, V. Sayseng, and E. E. Konofagoou, IEEE Trans. Ultrason. Ferroelectr. Freq. Control **64**, 1212 (2017).
24) Y. Honjo, H. Hasegawa, and H. Kanai, Proc. IEEE Int. Ultrason. Symp. 2008, p. 1995.
25) M. Couade, M. Pernot, M. Tanter, E. Messas, A. Bel, M. Ba, A.-A. Hagège, and M. Fink, IEEE Int. Ultrason. Symp. 2009, p. 515.
26) N. Furusawa, S. Mori, M. Arakawa, and H. Kanai, Proc. Symp. Ultrason. Electr. **39**, 1J1 (2018).
27) H. Kanai, M. Sato, Y. Koiwa, and N. Chubachi, IEEE Trans. Ultrason. Ferroelectr. Freq. Control **43**, 791 (1996).
28) H. Kanai, H. Hasegawa, Y. Koiwa, and M. Tanaka, IEEE Trans. Ultrason. Ferroelectr. Freq. Control **44**, 752 (1997).
29) H. Kanai, Ultrason. Med. & Biol. **35**, 936 (2009).
30) H. Hasegawa, Jpn. J. Appl. Phys. **56**, 07JF02 (2017).